



OPEN

Conversion of multilayer graphene into continuous ultrathin sp^3 -bonded carbon films on metal surfacesSUBJECT AREAS:
SURFACES, INTERFACES
AND THIN FILMS

GRAPHENE

Dorji Odkhoo¹, Dongbin Shin², Rodney S. Ruoff³ & Noejung Park^{1,2}Received
20 September 2013Accepted
4 November 2013Published
20 November 2013Correspondence and
requests for materials
should be addressed to
N.P. (noejung@unist.
ac.kr)

¹Interdisciplinary School of Green Energy and Low Dimensional Carbon Materials Center, ²Department of Physics, Ulsan National Institute of Science and Technology (UNIST), Ulsan 689-798, Korea, ³Department of Mechanical Engineering and the Materials Science and Engineering Program, The University of Texas, Austin, Texas 78712.

The conversion of multilayer graphenes into sp^3 -bonded carbon films on metal surfaces (through hydrogenation or fluorination of the outer surface of the top graphene layer) is indicated through first-principles computations. The main driving force for this conversion is the hybridization between sp^3 orbitals and metal surface d_z^2 orbitals. The induced electronic gap states and spin moments in the carbon layers are confined in a region within 0.5 nm of the metal surface. Whether the conversion occurs depend on the fraction of hydrogenated (fluorinated) C atoms at the outer surface and on the number of stacked graphene layers. In the analysis of the Eliashberg spectral functions for the sp^3 carbon films on a metal surface that is diamagnetic, the strong covalent metal- sp^3 carbon bonds induce soft phonon modes that predominantly contribute to large electron-phonon couplings, suggesting the possibility of phonon-mediated superconductivity. Our computational results suggest a route to experimental realization of large-area ultrathin sp^3 -bonded carbon films on metal surfaces.

Diamond is known for its extraordinary thermal conductivity and mechanical hardness, and the production of large-area crystals has been a long term goal. The conventional synthetic methods employed for the production of artificial diamond usually require extremely high pressure and temperature^{1,2}, or plasma-enhanced chemical vapor deposition (CVD)³⁻⁵. Advances in the growth of large-area graphene^{6,7} and bilayer graphene through multilayer graphenes⁸⁻¹⁰ suggest another possibility: the chemical conversion of a few layers of graphene into sp^3 -bonded carbon films. For example, previous theoretical results showed that the complete hydrogenation¹¹ or fluorination¹² of a single-layer of graphene can yield a thermodynamically stable sp^3 -bonded carbon layer. Indeed, partial hydrogenation of monolayer graphene^{13,14} and evidence of complete fluorination of monolayer graphene membranes¹⁵ have been experimentally achieved. Similarly, the conversion of a few layers of graphene has attracted attention, and hydrogenation of the outer surfaces of bilayer graphene^{16,17} to achieve all sp^3 -bonded carbon films has been treated theoretically. We suggest however that such an approach will be challenging experimentally as extensive hydrogenation or fluorination was stated to be needed on both the top and bottom surfaces.

Here we present a promising alternative, namely the conversion of graphene layers on a metal surface into sp^3 carbon films through surface hydrogenation or fluorination. From the practical point of view, the commonly used methods for growing graphene films on a metal substrate, either through CVD or as a result of the transfer of grown graphenes^{6-10,18}, are already providing appropriate target systems for the study of the sp^2 to sp^3 conversion of carbon films on metal surfaces. Our computation results suggest a method of preparing an ultrathin 'diamond' layer over even very large area by conversion of appropriate multilayer graphene on metal surfaces. The resulting structure could also be viewed as a carbon-based metal-insulator junction that may reveal novel two-dimensional (2D) phenomena, as we suggest in this study, or as a new type of electronic material¹⁹.

Results

We first investigated the effect of hydrogenation or fluorination on the free surface of the AB-stacked (Bernal-type stacking) bilayer graphene. Simulating experimental generation of gas phase atoms^{13,20}, hydrogen or fluorine atoms were considered to be available on the surface. Figure 1a is a schematic of the bilayer graphene before the adsorption of such gas atoms (denoted by I). Experimental studies reported that the hydrogen chemisorption coverage of a single-layer graphene is less than half of the carbon atoms²⁰. It was however suggested that bilayer or

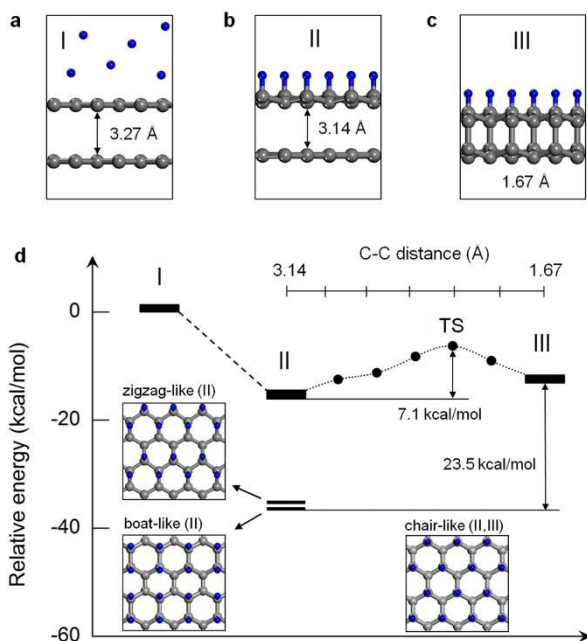


Figure 1 | The energetics related to the adsorption-induced geometric changes of bilayer graphene. The geometry (a) before (group I) and (b) after the hydrogen adsorption (group II), and (c) after formation of interlayer C–C bonds (group III). (d) Relative energies for each configuration and the energy barrier in unit of kcal mol^{-1} of hydrogen adatoms. The insets in (d) show three different atomic arrangements of hydrogen adsorption on the outer surface of graphene (boat-like, zigzag-like, and chair-like) in the group II. Only the chair-like configuration is available in the group III with an energy of about $23.5 \text{ kcal mol}^{-1}$ higher than that of the boat-like configuration in II. TS represents the transition state. The larger gray and smaller blue balls represent the carbon and hydrogen atoms, respectively.

multilayer graphene can have more extensive hydrogenation, which can be up to half the coverage of the outer surfaces^{16,21}. In Fig. 1, our super-cell model contains hydrogen (fluorine) atoms that could cover half the carbon atoms on the outer surface. After the chemisorption of hydrogen (fluorine) atoms, the two graphene layers can be separated by the ‘van der Waals’ (vdW) distance, as shown in Fig. 1b, or can form interlayer C–C bonds, as shown in Fig. 1c. The overall energetics for the cases of hydrogen adsorption is described in Fig. 1d.

The half coverage hydrogenation of the surface of graphene can exist in various configurations. Top views of the patterns, named as ‘boat-like’, ‘zigzag-like’, and ‘chair-like’^{11,12}, are presented in the insets of Fig. 1d. In the boat-like configuration, two hydrogen atoms are located at the two ends of the bridge of the C–C bond. In the zigzag-like configuration, each carbon atom in every second zigzag chain is bonded to a hydrogen atom. In the chair-like configuration, the C–H bonds are equally spaced. These three configurations, in which the carbon layers are separated by the vdW distance, are together categorized as configuration II in Fig. 1. Only the chair-like configuration induces all-carbon sp^3 hybridization in the carbon atoms, leading to sp^3 dangling bonds on the inner side of the top graphene layer. This drives formation of covalent C–C bonds between the upper and lower graphene layers, as shown in Fig. 1c (denoted as III). In contrast, dangling bonds are essentially not present for the boat-like and zigzag-like configurations owing to the pairing of two neighboring p orbitals in the form of local π bonding²². Thus, the boat-like and zigzag-like configurations are much more stable than the chair-like one either in the configuration II or III. Overall, the energetics shown in Fig. 1 indicate that the interlayer C–C bonds are not favored. Previously, it was shown that

hydrogenation of only one side of graphene can cause the graphene to roll-up²³. Such a structural instability of a flat graphene upon one-side hydrogenation further reduces the chance for the formation of interlayer C–C bonds.

When the one-side hydrogenated graphene bilayer is positioned on transition metal surfaces, the energetics for conversion to sp^3 films are significantly different than for the isolated bilayer case. In Fig. 2, we consider the same adsorption-induced conversion of bilayer graphene on the (0001) surface of Co (a few other metals are also considered, as discussed below). Besides the existence of Co below the graphene layers, the adsorption configurations of C–H bonds presented in Figs. 2a, b, and c, and the insets of Fig. 2d (configurations I, II, and III) are the same as those shown in Fig. 1. The favored adsorption site of carbon atoms is found to be atop Co atoms at the interface, as shown in Fig. 2a, which agrees with previous studies^{24,25}. The formation energy differences between the boat-like, zigzag-like, and chair-like configurations in group II are nearly the same as those presented in Fig. 1. However, it is noteworthy that the presence of Co greatly stabilizes the configuration III; this is in obvious contrast to the situation without the metal substrate. This stabilization occurs because of the saturation of the otherwise unstable sp^3 dangling bonds with Co surface states. Further, as shown in Fig. 2d, the transition barrier from configuration II to configuration III is negligibly small (about $0.5 \text{ kcal mol}^{-1}$).

Bond lengths and bond angles in configuration III reveal obvious sp^3 carbon (diamond-like) bond features. The calculated interlayer C–C and intralayer C–C bond lengths are 1.58 \AA and 1.52 \AA , respectively, and these values are comparable to the sp^3 bond length (1.54 \AA) in bulk diamond. The tetrahedral angles of the C–C–C bond within the layer and that formed with the interlayer C–C bond are 110.2° and 108.5° , respectively; these values are close to the tetrahedral bond angle of 109.5° . Fluorination of the graphene bilayer on Co(0001)

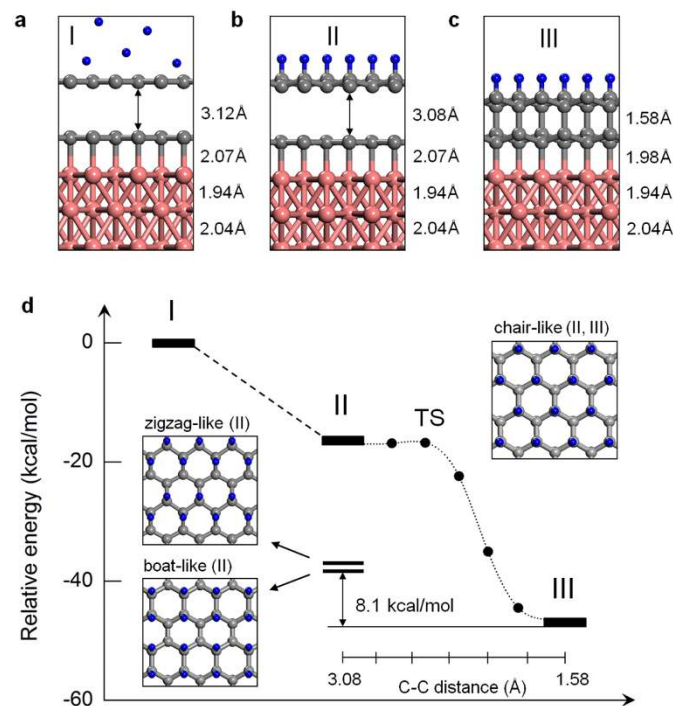


Figure 2 | The energetics of conversion of bilayer graphene into sp^3 carbon film on metal surface. (a–d) The same energetics and geometric changes as the ones that were shown in Fig. 1 but with Co(0001) underneath the graphene bilayer. In contrast to the cases of Fig. 1, the configuration III (the chair-like adsorption) is now more stable than the boat-like configuration in II by an energy difference of about $8.1 \text{ kcal mol}^{-1}$. The pink balls are the cobalt atoms.



revealed similar features as those observed for the hydrogenated cases. The details of structural properties are provided in Supplementary Table S1 in the Supporting Information.

To understand the underlying electronic origin of the sp^2 to sp^3 conversion, we investigated the electronic structures of the converted sp^3 carbon films on Co(0001). The projected electronic band structure and the projected density of states (PDOS) of carbon atoms in the outermost layer are presented in Fig. 3a. Pristine single-layer graphene has the cone-like energy bands touching the Fermi level at the K point of the 2D Brillouin zone. Such characteristics, originating from the delocalized π electronic states, largely disappeared upon the conversion from sp^2 to sp^3 bonding. The top of the valence bands, in which the p_x and p_y orbital states are degenerate, and the bottom of the conduction band, which is characteristic of a non-degenerate p_z orbital state, are set far apart from each other, resulting in a direct gap of about 3.18 eV at the Γ point. The first-principles calculations yielded similar wide band gaps for graphane^{11,12} and diamane^{16,26} (which are sp^3 carbon structures with full hydrogenation of top and bottom surfaces of graphene and AB-stacked bilayer graphene, respectively). The minority spin states, presented in Fig. 3b, reveal the same features; thus, there is no measurable magnetization in the outermost layer.

Figure 3c shows the band structure and PDOS in the majority spin state of the carbon layer at the interface with Co. The corresponding results for the minority spin states are shown in Fig. 3d. The in-plane p bands depicted in orange (p_x) and green (p_y) are almost identical to

the corresponding projected bands of the outer layer (Figs. 3a and b). However, the hybridization features between the carbon p_z and cobalt d_{z^2} orbitals are prominent throughout the energy level, leading to the drastic changes in energy and dispersion of p_z bands. For comparison, the projected electronic structures of majority and minority spins in the interface Co atoms are presented in Figs. 3e and f, respectively. Such strong hybridization causes exchange-splitting in the carbon layer. The magnetic moment in the first carbon layer is calculated to be about $-0.08 \mu_B$ per carbon atom and anti-parallel to the Co spin direction, which is twice the value observed in experiments for graphene adsorbed onto the Co(0001) surface²⁷. These metallic states developed at the interface can penetrate into the sp^3 carbon layers near the interface, constituting the metal-induced gap state (MIGS), as discussed in the next paragraph.

To estimate the range of the MIGS, we considered the possibility of converting graphene multilayers of various thickness (see further discussion on thickness-dependent energetics below) to sp^3 carbon films; for example, we considered the case of five graphene layers stacked in the AB configuration on Co(0001), as shown in Supplementary Fig. S1a. The PDOS resolved into each layer (see Supplementary Fig. S1c) shows that the first carbon layer (L1) at the interface with Co has electronic states persisting over the Fermi level with large exchange-splitting. The evanescent tails of such gap states decay rapidly and almost disappear in the third layer (L3). This indicates that such sp^3 C films with a thickness of only approximately 0.5 nm from the metal surface can likely provide good electric isolation.

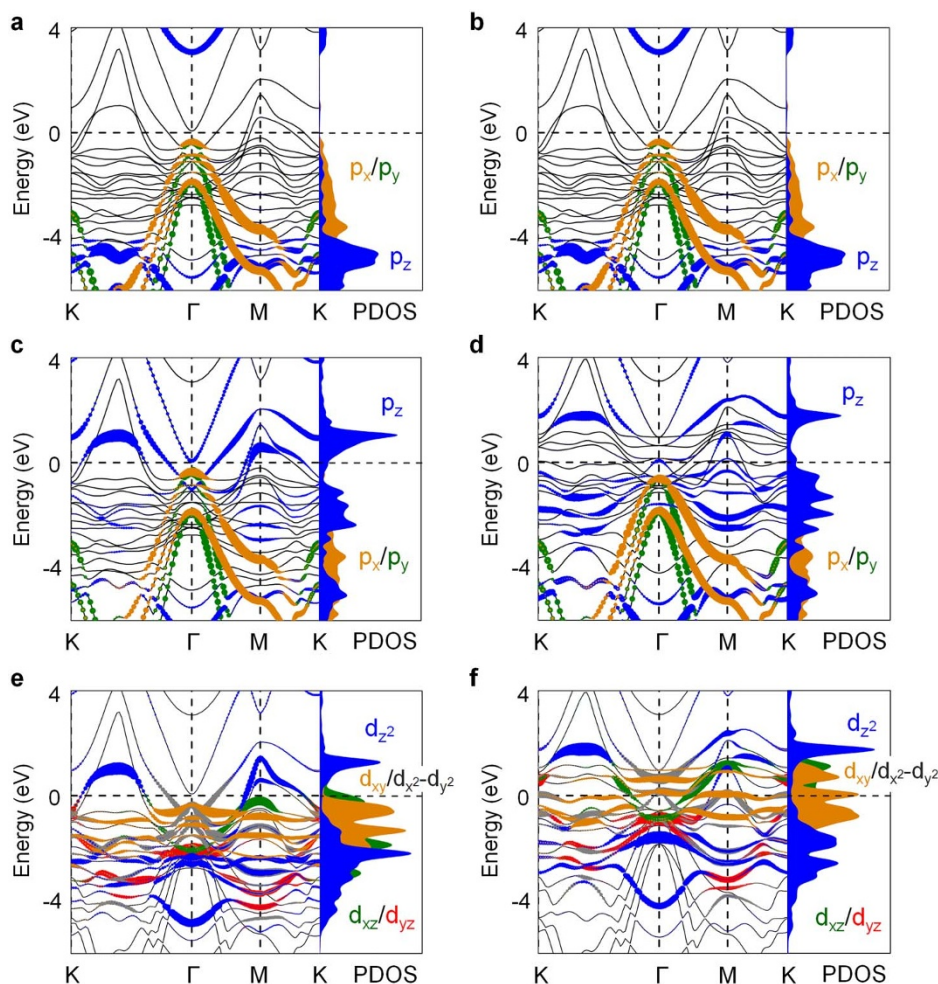


Figure 3 | Electronic structures of the two-layer sp^3 carbon film on Co(0001). (a) Majority and (b) minority spin band structures and PDOS of carbon atoms on the top layer. The same (c) majority and (d) minority states projected onto carbon atoms at the interface. The same (e) majority and (f) minority states projected onto the top Co layer at the interface. The Fermi level is set to zero energy.



We next investigated the effect of the coverage of hydrogen on the transformation of AB-stacked graphene bilayer into an sp^3 carbon film. Figure 4a shows the formation energy (solid circles) and interlayer distance (open circles) between the two graphene layers on Co(0001) as a function of the hydrogen coverage x of the outer (i.e., top) surface. The magnitude of the formation energy increases gradually with the coverage. A similar trend was observed previously in diamane structures¹⁶. The interlayer distance changes dramatically at around $x = 1/3$, as the interlayer C–C bonds develop at a higher concentration, whereas the two carbon layers remain at the vdW distance at a lower concentration. In Fig. 4a, to provide a generic model for the effect of the distribution of hydrogen adatoms, we assumed that the hydrogen adsorbates are distributed uniformly over the graphene surface. In realistic situations, there can be various other configurations with a given concentration. An example is provided in Fig. S2 in the Supporting Information. With the same concentration of $x = 1/6$, hydrogen adsorbates can be aggregated in a narrow region (Fig. S2a) or scattered uniformly (Fig. S2b). In the aggregated region ($x = 1$), the hydrogen adsorbates induce the C–C interlayer (sp^3) bonds in that region. This is consistent with the right side ($x > 1/3$, highly concentrated region) of Fig. 4a. Various adsorption configurations, within the same adatom concentration, can lead to various total energies, as demonstrated in Supplementary Fig. S3. However, the effect of local distribution of hydrogen adsorbates can be described by the model given in Fig. 4a. When the coverage of the outer surface is less than one quarter of the maximal coverage ($x = 0.25$ or C_8H), the two carbon layers are separated by 3.12 Å, which is essentially the interlayer vdW distance. For H coverage greater than half of the maximal coverage ($x = 0.5$ or C_4H), the formation of the interlayer C–C covalent bonds is favored, and the carbon atoms on both layers predominantly have the sp^3 characteristics. This dependence on the coverage is largely consistent with Angus and Hayman's formulation²⁸ for the composition of sp^3 and sp^2 bonds in hydrogen-treated diamond-like hydrocarbons, as discussed in detail in the Supplementary Information.

We now report the effect of thickness on the stability of fully hydrogenated (C_2H) sp^3 carbon films on metal substrates. We consider two different stacking configurations of graphene layers, namely ABC and AA. The ABC-stacked graphene was converted

into a cubic diamond-like layer, whereas the AA-stacked graphene transformed into a hexagonal diamond-like layer. The side views of the cubic and hexagonal diamond-like overlayers are presented in the insets of Fig. 4b: the cubic diamond consists of three alternating layers (denoted by α , β , and γ) and the hexagonal diamond consists of two alternating layers (denoted by α and β). Figure 4b shows the formation energies of cubic and hexagonal diamond-like ultrathin films on the Co(0001) substrate. The negative formation energies indicate that the sp^3 -bonded diamond-like structures on the Co surface are thermodynamically and structurally stable for thicknesses of up to seven carbon layers.

The preferable conversion energetics from sp^2 layers into sp^3 carbon films can be applied to the cases of other metal surfaces. The reactivity of metal surfaces can be roughly classified into two groups, depending on the strength of their interaction with graphene: the 'physisorption group' (e.g., Cu, Pt, Al, Ag, or Au), corresponding to the surfaces on which graphene weakly physisorbs through vdW attraction, and the 'chemisorption group' (e.g., Ni, Co, or Pd), corresponding to the surfaces on which graphene develops relatively strong chemical bonds through a hybridization between its p orbitals and the metal d orbitals²⁴. In the present study, we selected Co(0001), Ni(111), and Cu(111) because of the convenience associated with the periodic super-cell calculation; the lattice mismatches of these metals with the graphene are only 1.6, 1.2, and 3.6%, respectively. As expected, the conversion energetics for graphene layers on Ni(111) revealed features that were almost similar to those of Co(0001).

A more remarkable point is the stabilization of the configuration III on the Cu(111) surface. As discussed in Ref. 24, the overlayer of pure graphene (configuration I) and the one-side hydrogenated graphenes (configurations II) physisorb onto Cu(111) through the vdW interaction. However, for configuration III, the sp^3 dangling bonds at the interface develop covalent bonds with surface Cu atoms, similar to that observed for Co and Ni. The calculated relative energies of the hydrogenated bilayer graphene on Ni(111) and Cu(111) substrates (along with the case of Co(0001) and the case without metal substrate) are summarized in Table 1. Clearly, *the stabilization by hybridization between the sp^3 dangling orbital and the d_z metallic orbital in configuration III applies not only to the chemisorbing metal surfaces, such as Co and Ni, but also to the relatively less reactive*

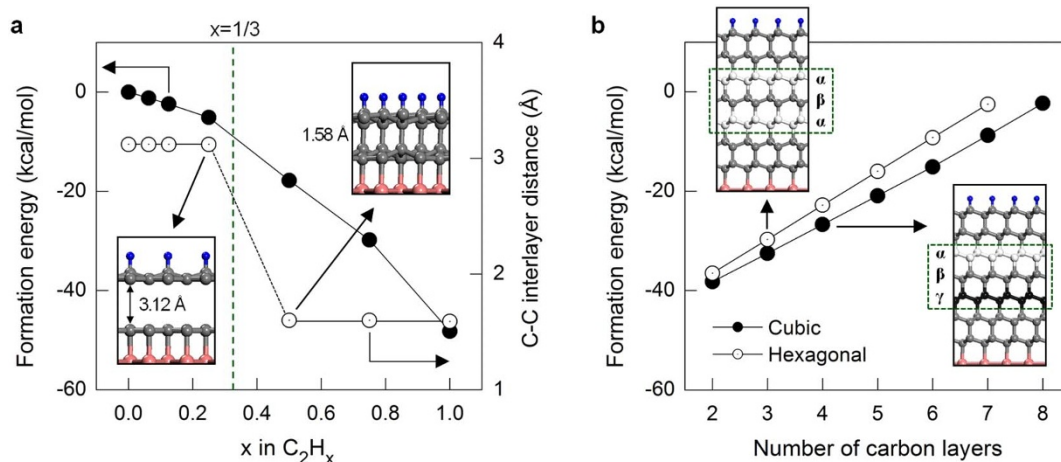


Figure 4 | The dependence of stability of sp^3 carbon films on the adsorption coverage and thickness. (a) The hydrogen coverage-dependent formation energy (solid circles) and optimized C–C interlayer distance (open circles) of bilayer graphene on Co(0001). The vertical dashed line represents the critical coverage ($x \approx 1/3$) beyond which the interlayer C–C bonds are predominantly favored. The insets show the optimized structures corresponding to the coverage just below ($x = 0.25$) and above ($x = 0.5$) the critical coverage. In this model, hydrogen adsorbates are distributed uniformly over the two-dimensional supercell. The definition of the formation energy is described in the Supplementary Information. (b) The thickness-dependent formation energies of the fully hydrogenated (C_2H at the outer surface) sp^3 carbon films on Co(0001). Solid and open symbols refer to the formation of cubic and hexagonal diamond configuration, respectively. The insets show the side views of the optimized seven-layer diamond-like films on Co. The carbon atoms in different stacking layers ($\alpha\beta\gamma$ for cubic and $\alpha\beta$ for hexagonal diamond configurations) are differentiated with gray scale. For simplicity, only the top-most Co layer is shown. Other atomic symbols follow the same convention used in Fig. 2.



Table 1 | Relative energies of configurations I, II, and III depicted in Figs. 2a, b, and c on Co(0001), Ni(111), and Cu(111), respectively. In each case with different metal, the energy reference is the configuration I. The energies are given in kcal mol⁻¹ of hydrogen adatoms.

Groups	Configurations	Pristine	Cobalt	Nickel	Copper
I	–	0.0	0.0	0.0	0.0
	boat-like	–36.4	–37.3	–37.1	–38.1
II	zigzag-like	–35.4	–36.5	–36.2	–37.2
	chair-like	–15.6	–16.2	–16.4	–18.8
III	chair-like	–12.9	–45.4	–47.8	–45.2

metals, such as Cu. Very recently, Rajasekaran *et al.*²⁹ reported experimental evidence for the partial conversion of a few layer graphene to sp³-bonded carbon layers on Pt(111) substrate.

The electronic structures of the sp³-bonded carbon layers on metal surfaces shown above revealed similar features as those of hole-doped diamond. This motivated us to study the features of electron-phonon coupling that may lead to phonon-mediated superconductivity. The superconductivity of hole-doped diamond (the substitution of B for C) has attracted broad interest^{30,31}, and a possible modulation of critical temperature (T_c) in a single sp³ carbon layer (i.e., graphene) through B doping has also been studied recently³². To investigate the electron-phonon coupling characteristics in the metal/diamond interface structures, we selected a two-layer sp³ carbon structure on Cu(111) that possesses a perfect diamagnetic electronic structure. The phonon DOS (PHDOS) of the hydrogenated sp³-bonded carbon layers on Cu(111) is shown in Fig. 5a. For comparison, the PHDOS of the two-layer sp³ structure hydrogenated on both sides (i.e., diamane) is also presented in Fig. 5a. Both systems show quite similar PHDOS characteristics in the frequency modes ranging from 400 to 1300 cm⁻¹; the overall patterns are analogous to those of pristine diamond³³. The sharp peaks around 1200–1300 cm⁻¹ can mainly be attributed to the shear motion between the carbon and hydrogen layer in the outer surface. The C–C in-plane and out-of-plane vibrations dominate the medium-frequency region, contributing to peaks at around 600, 800, and 1000 cm⁻¹. Details on the optical phonon modes are given in Supplementary Fig. S4 in the Supporting Information. For the cases of B-doped graphene and diamonds, the softening of these carbon stretching modes with increasing doping concentration has been discussed in relation to the electron-phonon coupling strength that is a key component determining T_c ^{32,34}. By comparison with the diamane, a PHDOS characteristic of the sp³ layer on Cu is the presence of soft modes in the frequency range below 250 cm⁻¹ that are due to the vibration of Cu–C bonds: in-plane modes with a peak at about 140 cm⁻¹ and out-of-plane modes with a peak at about 230 cm⁻¹ (indicated by arrows).

Figure 5b shows the Eliashberg's spectral function $\alpha^2F(\omega)$ and the electron-phonon coupling constant calculated for the sp³-bonded carbon layers on Cu(111). Here, $\lambda(\omega)$ is defined as

$$\lambda(\omega) = 2 \int_0^{\omega} \frac{\alpha^2F(\omega')}{\omega'} d\omega',$$

and thus the total electron-phonon coupling constant is $\lambda(\omega \rightarrow \infty)$. The overall PHDOS characteristics dominate the $\alpha^2F(\omega)$ throughout the range of phonon frequencies. The calculated $\lambda(\omega)$ increases in two steps at low and medium frequencies, at which the aforementioned Cu–C and C–C modes exert a critical effect. More specifically, $\alpha^2F(\omega)$ possesses a sizeable spectrum (indicated by an arrow) at the low frequency region, that extends up to 250 cm⁻¹, which can be attributed to soft phonons of the metal/sp³ carbon interface, which contribute considerably to the integrated λ of 0.25. The high-frequency peaks in $\alpha^2F(\omega)$ at around 1200–1300 cm⁻¹, originated from the shear motion of the outermost C and H layers, provides a negligible contribution to λ ³², because the integrand is the inverse of ω .

As a complementary study, in order to compare with the B-doped diamond systems, we also considered the effect of hole-doping on λ .

As is summarized in Supplementary Table S2, the quantity λ increases with increasing B doping concentration and reaches 0.81 at the doping concentration of 12.5%, which is substantially greater than the value of 0.56 obtained for a 10% B-doped diamond³⁴. This sharp increase in λ is mainly attributed to the enhancement of the electronic DOS at the Fermi level ($N(E_F)$). *These results imply that the λ value can be engineered by choosing the metal substrate that can promote $N(E_F)$ to the interface sp³ carbon layers.* To demonstrate this conjecture, we repeated our calculations for the sp³-bonded carbon layers on the (111) surface of Pt: the relatively large $N(E_F)$ indeed leads to a large λ of 0.45 *without doping* (see Supplementary Table S2).

The computation for a thicker sp³ carbon layer on metal surface is quite demanding, but we suggest that the results of electron-phonon calculations presented above should be valid for thicker diamond layers because the σ -bonded Fermi level states in the sp³ framework are rather localized in the vicinity of the metal/diamond interface. To verify the accuracy of the present computation, we calculated the

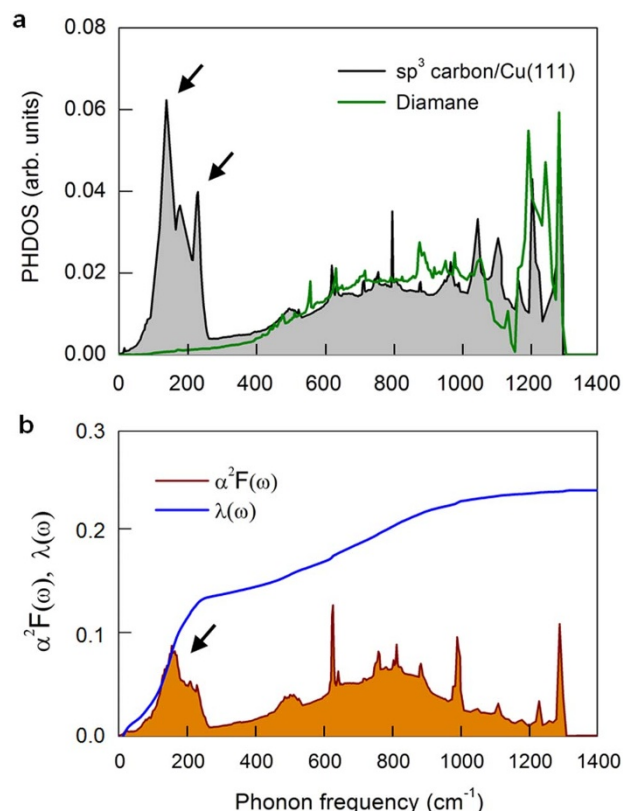


Figure 5 | Phonon and electron-phonon coupling features of the sp³ carbon/Cu(111) interface. (a) PHDOS and (b) Eliashberg spectral function $\alpha^2F(\omega)$ and the electron-phonon coupling constant $\lambda(\omega)$ for the two-layer sp³ carbon film on Cu(111). In (a), the PHDOS for diamane is shown with the green line for comparison. The arrows indicate the C–Cu vibration modes.



electron-phonon features of known materials (i.e., MgB₂) and the results with references are shown in Table S2 in the Supporting Information. For the case of the sp² graphene overlayer on Cu(111), λ is quite small, and thus the possibility of phonon-mediated superconductivity is negligible. This is almost the same situation as the pristine single-layer and bilayer graphenes, as discussed in the previous first-principles study³⁵. Even though the calculated λ and T_c of our sp³ carbon layers on metals are lower than those of MgB₂, our results indicate that metal/sp³ carbon interfaces are a new candidate for superconductivity studies.

Discussion

Through the first-principles density functional theory (DFT) calculations, we investigated the energetics of transformation of a few layers of graphene into sp³-bonded thin overlayers on metallic surfaces (Co, Ni, and Cu). Strong hybridization between the sp³ dangling bonds orbitals and the metallic surface d_{z²} orbitals stabilizes the sp³-bonded carbon layers. The dependence of the energetics of conversion on the surface coverage of C–H or C–F bonds and on the thickness of the stacked graphene layers was tabulated. Phonon spectra were calculated, and the features of electron-phonon coupling with the possibility of superconductivity were investigated through analyses of the Eliashberg's spectral function. Our results suggest that scaled preparations of multilayer graphene on metal substrates can lead to a fabrication route of very large area ultrathin sp³-bonded carbon films that would represent an entirely new carbon material.

Methods

The DFT calculations were performed using the projector augmented wave pseudo-potential method³⁶, as implemented in the Vienna Ab initio Simulation Package³⁷. Exchange and correlation interactions between electrons were described with the generalized gradient approximation formulated by Perdew, Burke, and Ernzerhof³⁸. The long-range dispersion corrections for the interlayer interaction were taken into account within the semi-empirical DFT-D2 approach suggested by Grimme³⁹. Spin polarization was taken into account for all the calculations. Some more details for supercell configurations, relaxation scheme, and k-point samplings are given in the Supplementary Information.

The PHDOS, Eliashberg spectral function $\alpha^2F(\omega)$, and electron-phonon coupling $\lambda(\omega)$ were calculated using the linear response theory within the density functional perturbation theory⁴⁰, as implemented in the Quantum ESPRESSO⁴¹. The critical temperature T_c was estimated using McMillan's formula for the Eliashberg equation⁴²,

$$T_c = \frac{\omega_{in}}{1.2} \exp \left[\frac{-1.04(1+\lambda)}{\lambda(1-0.62\mu^*) - \mu^*} \right], \quad (1)$$

where ω_{in} is the logarithmic average frequency and μ^* is the screened Coulomb pseudo-potential. The values of T_c shown in Supplementary Table S2 in Supporting Information were calculated with the typical choice of $\mu^* = 0.1^34$.

- Bundy, F. P., Hall, H. T., Strong, H. M. & Wentorf Jun, R. H. Man-made diamonds. *Nature* **176**, 51–55 (1955).
- Irifune, T., Kurio, A., Sakamoto, S., Inoue, T. & Sumiya, H. Materials: Ultrahard polycrystalline diamond from graphite. *Nature* **421**, 599–600 (2003).
- Bachmann, P. K., Leers, D. & Lydtin, H. Towards a general concept of diamond chemical vapour deposition. *Diamond Relat. Mater.* **1**, 1–12 (1991).
- Isberg, J. *et al.* High carrier mobility in single-crystal plasma-deposited diamond. *Science* **297**, 1670–1672 (2002).
- Butler, J. E. & Sumant, A. V. The CVD of nanodiamond materials. *Chem. Vap. Deposition* **14**, 145–160 (2008).
- Li, X. *et al.* Large-area synthesis of high-quality and uniform graphene films on copper foils. *Science* **324**, 1312–1314 (2009).
- Bae, S. *et al.* Roll-to-roll production of 30-inch graphene films for transparent electrodes. *Nature Nanotech.* **5**, 574–578 (2010).
- Wu, Y. *et al.* Growth mechanism and controlled synthesis of AB-stacked bilayer graphene on Cu–Ni alloy foils. *ACS Nano* **6**, 7731–7738 (2012).
- Li, Q. *et al.* Growth of adlayer graphene on Cu studied by carbon isotope labeling. *Nano Lett.* **13**, 486–490 (2013).
- Chen, S. *et al.* Synthesis and characterization of large-area graphene and graphite films on commercial Cu–Ni alloy foils. *Nano Lett.* **11**, 3519–3525 (2011).
- Sofa, J. O., Chaudhari, A. S. & Barber, G. D. Graphane: A two-dimensional hydrocarbon. *Phys. Rev. B* **75**, 153401 (2007).
- Leenaerts, O., Peelaers, H., Hernández-Nieves, A. D., Partoens, B. & Peeters, F. M. First-principles investigation of graphene fluoride and graphane. *Phys. Rev. B* **82**, 195436 (2010).

- Elias, D. C. *et al.* Control of graphene's properties by reversible hydrogenation: Evidence for graphane. *Science* **323**, 610–613 (2009).
- Balog, R. *et al.* Nature Mater. **9**, 315–319 (2010).
- Robinson, J. T. *et al.* Properties of fluorinated graphene films. *Nano Lett.* **10**, 3001–3005 (2010).
- Leenaerts, O., Partoens, B. & Peeters, F. M. Hydrogenation of bilayer graphene and the formation of bilayer graphane from first principles. *Phys. Rev. B* **80**, 245422 (2009).
- Samarakoon, D. K. & Wang, X. Q. Tunable band gap in hydrogenated bilayer graphene. *ACS Nano* **4**, 4126–4130 (2010).
- Kim, K. S. *et al.* Large-scale pattern growth of graphene films for stretchable transparent electrodes. *Nature* **457**, 706–710 (2009).
- Ruoff, R. S. Personal perspectives on graphene: New graphene-related materials on the horizon. *MRS Bull.* **37**, 1314–1318 (2012).
- Rajasekaran, S. *et al.* Reversible graphene-metal contact through hydrogenation. *Phys. Rev. B* **86**, 075417 (2012).
- Luo, Z. Q. *et al.* Thickness-dependent reversible hydrogenation of graphene layers. *ACS Nano* **3**, 1781–1788 (2009).
- Han, S. S., Jung, H., Jung, D. H., Choi, S. H. & Park, N. Stability of hydrogenation states of graphene and conditions for hydrogen spillover. *Phys. Rev. B* **85**, 155408 (2012).
- Neek-Amal, M., Beheshtian, J., Shayeghanfar, F., Singh, S. K., Los, J. H. & Peeters, F. M. Spiral graphone and one-sided fluorographene nanoribbons. *Phys. Rev. B* **87**, 075448 (2013).
- Giovannetti, G. *et al.* Doping graphene with metal contacts. *Phys. Rev. Lett.* **101**, 026803 (2008).
- Eom, D. *et al.* Structure and electronic properties of graphene nanoislands on Co(0001). *Nano Lett.* **9**, 2844–2848 (2009).
- Chernozatonskii, L. A., Sorokin, P. B., Kvashnin, A. G. & Kvashnin, D. G. Diamond-like C₂H nanolayer, diamane: Simulation of the structure and properties. *JETP Lett.* **90**, 134–138 (2009).
- Rader, O. *et al.* Is there a rashba effect in graphene on 3d ferromagnets? *Phys. Rev. Lett.* **102**, 057602 (2009).
- Angus, J. C. & Hayman, C. C. Low-pressure, metastable growth of diamond and “diamondlike” phases. *Science* **241**, 913–921 (1988).
- Rajasekaran, S., Abild-Pedersen, F., Ogasawara, H., Nilsson, A. & Kaya, S. Interlayer carbon bond formation induced by hydrogen adsorption in few-layer supported graphene. *Phys. Rev. Lett.* **111**, 085503 (2013).
- Ekimov, E. A. *et al.* Superconductivity in diamond. *Nature* **428**, 542–545 (2004).
- Lee, K. W. & Pickett, W. E. Superconductivity in boron-doped diamond. *Phys. Rev. Lett.* **93**, 237003 (2004).
- Savini, G., Ferrari, A. C. & Giustino, F. First-principles prediction of doped graphane as a high-temperature electron-phonon superconductor. *Phys. Rev. Lett.* **105**, 037002 (2010).
- Pavone, P. *et al.* Ab initio lattice dynamics of diamond. *Phys. Rev. B* **48**, 3156–3163 (1993).
- Boeri, L., Kortus, J. & Andersen, O. K. Three-dimensional MgB₂-type superconductivity in hole-doped diamond. *Phys. Rev. Lett.* **93**, 237002 (2004).
- Park, C. H., Giustino, F., Cohen, M. L. & Louie, S. G. Electron-phonon interactions in graphene, bilayer graphene, and graphite. *Nano Lett.* **8**, 4229–4233 (2008).
- Blöchl, P. E. Projector augmented-wave method. *Phys. Rev. B* **50**, 17953–17979 (1994).
- Kresse, G. & Hafner, J. Ab initio molecular-dynamics for liquid-metals. *Phys. Rev. B* **47**, 558–561 (1993).
- Perdew, J. P., Burke, K. & Ernzerhof, M. Generalized gradient approximation made simple. *Phys. Rev. Lett.* **77**, 3865–3868 (1996).
- Grimme, S. Semiempirical GGA-type density functional constructed with a long-range dispersion correction. *J. Comput. Chem.* **27**, 1787–1799 (2006).
- Baroni, S., de Gironcoli, S., Dal Corso, A. & Giannozzi, P. Phonons and related crystal properties from density-functional perturbation theory. *Rev. Mod. Phys.* **73**, 515–562 (2001).
- Giannozzi, P. *et al.* QUANTUM ESPRESSO: a modular and open-source software project for quantum simulations of materials. *J. Phys.: Condens. Matter* **21**, 395502 (2009).
- McMillan, W. L. Transition temperature of strong-coupled superconductors. *Phys. Rev.* **167**, 331–344 (1968).

Acknowledgments

This research was supported by the Basic Science Research Program through the National Research Foundation of Korea (NRF), funded by the Ministry of Education (NRF-2013R1A1A2007910). R.S.R. appreciates support by his Cockrell Family Endowed Regents Chair.

Author contributions

D.O. performed the calculations and prepared the manuscript. D.S. carried out the electron-phonon coupling calculations. R.S.R. contributed scientific ideas and guidance including on the contents/preparation of the manuscript. N.P. designed research and helped define content of the manuscript. All authors have given approval to the final version of the manuscript.



Additional information

Supplementary information accompanies this paper at <http://www.nature.com/scientificreports>

Competing financial interests: The authors declare no competing financial interests.

How to cite this article: Odkhuu, D., Shin, D., Ruoff, R.S. & Park, N. Conversion of multilayer graphene into continuous ultrathin sp^3 -bonded carbon films on metal surfaces. *Sci. Rep.* 3, 3276; DOI:10.1038/srep03276 (2013).



This work is licensed under a Creative Commons Attribution-NonCommercial-ShareAlike 3.0 Unported license. To view a copy of this license, visit <http://creativecommons.org/licenses/by-nc-sa/3.0>